Journal of Applied Polymer Science

Influence of hygrothermal aging on dimensional stability of thin injection-molded short glass fiber reinforced PA6 materials

Thomas Illing,[1] Marcus Schoßig,[2] Christian Bierögel,[2,3] Wolfgang Grellmann[2,3]
[1]Valeo Schalter und Sensoren GmbH, Bietigheim-Bissingen 74321, Germany
[2]Polymer Service GmbH Merseburg, Merseburg 06217, Germany
[3]Center of Engineering Sciences, Martin-Luther University Halle-Wittenberg, Halle (Saale) 06099, Germany
Correspondence to: T. Illing (E-mail: thomas.illing@valeo.com)

ABSTRACT: The hygrothermal aging of short glass fiber reinforced polyamide 6 materials (PA6/GF) is a major problem for thin-walled components used in the automotive sector. In this work, the thickness and glass fiber content of PA6/GF materials were varied and exposed to hygrothermal aging. The temperature and relative humidity were chosen to range from −40 to 85°C and 10% RH to 85% RH respectively, according to automotive requirements for components in the passenger compartment. For the absorption of moisture, the diffusion behavior could not be generally described by Fick's law. However, the results indicate that the diffusion behavior is dependent on the relative humidity and thickness of the PA6/GF material. The morphology of the test specimen, which is influenced by injection molding, was also found to affect the diffusion behavior. The states of equilibrium for moisture absorption are strongly dependent on the relative humidity during hygrothermal aging and less dependent on the temperature. The maximum absorbed humidity was found at a temperature of 65°C and 85% RH, which was higher than at 85°C and 85% RH because of reduced contrary aging processes, such as postcrystallization. In certain climatic conditions and test specimen thicknesses, there was a characteristic overshoot in the mass change. This behavior could be attributed to a different degree of crystallization and lower glass fiber content. Both moisture absorption and an overshoot of the mass affected the dimensional stability of the test specimens. This effect on dimensional stability could be correlated with the glass fiber orientation. © 2015 Wiley Periodicals, Inc. J. Appl. Polym. Sci. **2015**, *132*, 42245.

KEYWORDS: ageing; fibers; polyamides; structure; property relations

Received 7 August 2014; accepted 19 March 2015
DOI: 10.1002/app.42245

INTRODUCTION

Short glass fiber reinforced polyamide 6 materials (PA6/GF) have been successfully used for many decades in the automotive industry, especially for components in the exterior and interior areas. The advantageous combination of mechanical and thermal properties, together with a convenient production process that utilizes injection molding, allows a wide operational range and variable shaping. Due to product safety requirements in the automotive industry components are exposed to hygrothermal stress during the development phase. However, the current trend towards lighter weight components and less material consumption is leading to thinner walls in automotive components. At the same time demands for accuracy, tolerance and aging stability are increasing. This work aims to contribute to the broader understanding of the dimensional stability and the mechanical and thermal properties of short glass fiber reinforced polyamide 6 materials during the hygrothermal aging process.

The hygroscopic behavior of polyamide materials is generally well understood. For example, absorption of moisture in such materials has been well described.[1–3] Furthermore, the moisture absorption characteristics of polyamide materials have been correlated with a number of factors including temperature,[4–11] glass fiber content,[7,12] and thickness[13] of the specimen. These characteristics can be described by Fick's laws of diffusion and the resulting model by Crank and Park.[1] The model of Crank and Park describes the diffusion of water molecules in amorphous regions of the partially crystalline PA6. The mathematical relationship is given by eq. (1)

$$M_t = M_e - M_e \frac{8}{\pi^2} \sum_{k=1}^{20} \left(\frac{1}{2k+1}\right)^2 \cdot \exp\left[-\frac{Dt}{h^2}\pi^2(2k+1)^2\right] \quad (1)$$

where M_t is the actual mass, M_e the mass in the equilibrium state, k is the factor of the Taylor series, D is the diffusion coefficient, t is the time, and h is the thickness.

However, several different authors have observed an overshoot in the mass increase in semicrystalline materials.[14–16] Low *et al.*[14] have attributed the mass overshoot from moisture absorption to the following five factors: first, re-orientation of the molecular chains due to the ingress of moisture; second, moisture-induced crystallization; third, the forming processes of crystalline regions. Fourth, the relaxation of molecular chains to a more compact structure, and fifth, the dissolution of low molecular weight components from the polymer matrix. Due to the absorption of moisture the distances between the molecular chains increase, which inevitably affect the geometrical dimensions of the test specimens.[4,5,7,8] Furthermore, it is possible that glass fibers and their sizing, facilitate diffusion along the orientation direction.[5,6,13,17] The glass fiber content and orientation also influences the geometrical changes which are furthermore affected by the glass fiber content itself. Due to the absorption of water a decrease in strength and stiffness occur. For a detailed description of changes in mechanical properties as a function of water content the reader is referred to.[5,10,17–20] This characteristic material behavior, can be supported at higher temperatures due to chemical aging processes described by Kohan and Becker and Braun.[21,22] Such processes start to influence PA6 from a temperature of about 80°C. On the other hand, characteristic material behavior may be encumbered by counteracting physical aging processes such as post crystallization.[6,7] Compared to hydrothermal aging in water, in hygrothermal aging, the diffusion depends on the relative humidity and the temperature-dependent saturation vapor pressure must also be taken into account.[14,23,24] In contrast to the previous works, this paper takes relative humidity into account when determining the moisture absorption. Variations in the temperature, specimen thickness and the glass fiber content are also included in our analysis. Unlike hydrothermal aging, little attention has been paid to dimensional stability during the hygrothermal aging process. In particular, material characteristics related to the mass overshoot and dimensional stability have not been adequately addressed in the literature. In this paper the effect of moisture absorption on the dimensional stability of the test specimens were correlated with glass fiber orientation which was determined by computer tomography.

EXPERIMENTAL

Materials

In this work short glass fiber reinforced polyamide 6 (PA6/GF) and unreinforced polyamide 6 (PA6) were studied. The materials were provided by BASF SE, Ludwigshafen, Germany. In Table I, the tested materials and their respective glass fiber contents are listed.

Manufacturing of Test Specimen

For the investigations, plates with dimensions of 185 × 160 mm^2 were prepared by injection molding. Then six multipurpose test specimens of type 1A according to ISO 3167,[26] and four square specimens with dimensions of 60 mm by 60 mm according to ISO 294-3[27] (hereinafter named as squares, see Figure 1) were extracted from the plates by sawing and milling. This was done to evaluate the influence of the glass fiber orientation both along and transverse to the direction of injection molding. Figure 2 shows schematically the positions from where the multipurpose test specimens were removed from the injection molded plates. The film gate is indicated by a red arrow, and the fiber orientation by black dotted lines. Table II lists the materials tested with their respective thicknesses and glass fiber mass contents.

Table I. Investigated Materials from BASF SE

Matrix material	Glass fiber mass content Ψ (–)	Glass fiber volume content φ_V (–)	Material name
PA6	0	0	BASF Ultramid B3K[25]
PA6	0.15	0.067	BASF Ultramid B3EG3
PA6	0.30	0.159	BASF Ultramid B3EG6
PA6	0.40	0.243	BASF Ultramid B3G8

Hygrothermal Aging

Different temperatures and moisture contents were chosen to assess the influence of relative humidity and temperature on the properties of the PA6/GF materials. The selected parameters for the climate storages are listed together with the underlying standards in Table III. The climate storage took place for up to 1000 h, at defined time intervals of 24, 48, 96, 480, and 1000 h. Test specimens and squares were taken out to determine the dimensional change as well as the change of mass, density and enthalpy.

Evaluation of Property Changes

In order to evaluate the change in properties of the PA6/GF material, changes in mass, density, geometrical dimensions and differential scanning calorimetry (DSC) were analyzed for each climate storage condition. The mass was determined gravimetrically with an accuracy of ±1 mg on the squares and the density was determined by the measurement device SARTORIUS CP124S-0CE according to ISO 1183-1 method A.[31] The evaluation of the geometrical dimensions was carried out by means of the measuring microscope MITUTOYO QUICK SCOPE QS250Z-3D CNC VISION MEASURING MACHINE with an accuracy of ±2.5 µm. The change in the degree of crystallization was determined by the measurement device METTLER–TOLEDO DSC 820 according to ISO 11537-1 at a heating rate of 10 K/min within a temperature range of 0–300°C.[32] To assess the degree of crystallinity *K*, the enthalpy of fusion for 100% crystalline PA6 was selected, which has a value of 230 J/g.[33] The orientation of the glass fibers was analyzed by computed tomography (MicroCT) with the device GENERAL ELECTRIC NANOTOM M with a resolution of 4 µm and subsequent software analysis with VOLUME GRAPHICS STUDIO MAX V2.2.

RESULTS AND DISCUSSION

Relative Change of Mass at High Relative Humidity

The change in mass by absorption of moisture takes place in amorphous polymers usually according to Fick's 1st law, which describes the diffusion of foreign materials.[1–3] The diffusion is accelerated by a gradient, which is formed due to the difference in concentration of the two substances involved, see eq. (2).[34]

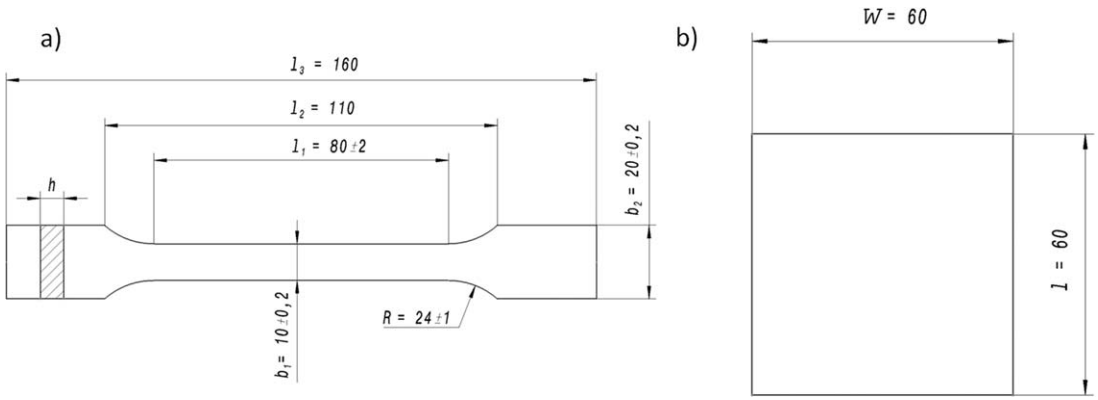

Figure 1. Drawing of used specimen according ISO 3167 (a) and ISO 294-3 (b), dimensions in mm.

$$\frac{dm}{dt} = -D \cdot A \cdot \frac{dc}{dx} \tag{2}$$

Here, *dm/dt* is the increase in mass as a function of time, *D* is the diffusion coefficient, *A* is the cross-sectional area, *c* is the concentration of the substance diffused into the component and *x* is the thickness. Figure 3 shows the relative increase in mass (Δm) as a function of glass fiber content, calculated according to eq. (3) for test specimen thicknesses of 1.5 and 4 mm for climate storage values of at 85°C and 85% RH.

$$\Delta m = \frac{m_t - m_{\text{start}}}{m_{\text{start}}} \cdot 100 \tag{3}$$

The fit curves of the respective Fick's mass increase, which are calculated according to eq. (1) are shown in Figure 3(a,b) as solid lines. The calculated parameters used in Figure 2 are listed in Table IV. It can be observed that measured values of the squares with a thickness of 4 mm conform to the empirical model regardless of the fiber content, whereas the 1.5 mm squares undergo a higher increase in mass than predicted in the first 96 h of climate storage. This increased mass gain depends on the fiber content, which will be discussed later on in this work in more detail. Furthermore, it can be established that at a thickness of 1.5 mm, no equilibrium state is reached, rather there is a slight decrease in mass with increasing time after reaching the maximum value (see Figure 3).

The calculated mass increases the equilibrium state of PA6 and PA6/GF40 are 4.2 and 2.5%, respectively. These values are slightly lower than the values of Valentin who has reported a mass increase of 5 and 3.5% for PA66 and PA66/GF40 respectively after storage of 3 mm thickness test specimen in water at 70°C.[12] As can be seen in Figure 3, the relative mass change is dependent on glass fiber content. Due to the fact that the glass fibers themselves do not absorb any moisture,[13] the increase of mass can be considered independent of fiber content and can be normalized according to eq. (4).

$$M_{t,\text{norm}} = \frac{M_t}{1 - \Psi} \tag{4}$$

It follows that in these climate conditions the absorption of relative humidity is determined by the polymer matrix, and the effect of the glass fiber content is very small; that is, no preferential uptake of moisture along glass fibers or in the fiber sizing was observed, unlike for example in Boukhoulda *et al.* who has reported these effects for long fiber reinforced composites.[35] At the same time, however, the glass fibers do not impede diffusion. A small difference in the normalized mass increase at a thickness of 4 mm with respect to the nonreinforced polymer matrix may be structurally related and suggests differences in morphology. It can be seen from Figure 3(a,b), that the equilibrium state of the moisture gain also depends on the thickness. Thus, the maximum moisture uptake at PA6/GF30 and 4 mm thickness is 2.7%. While the maximum value for 1.5 mm thickness is only 1.9%. This difference can also be seen in the diffusion coefficient *D*, which is greater at a thickness of 4 mm than at a thickness of 1.5 mm by an averaged factor of 1.3.

Dependence of the Relative Mass Change on the Content of Humidity

In Figure 4, PA6/GF30 squares with a thickness of 1.5 and 4 mm are exposed to a climate condition of 85°C and various levels of humidity. At the beginning of the climate storage,

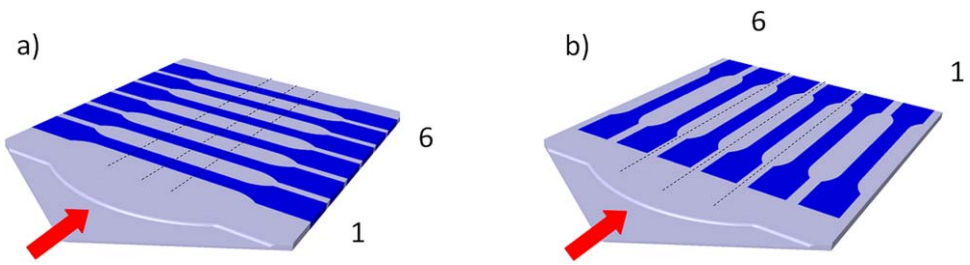

Figure 2. Schematic representation of the multipurpose test specimen, transverse (a) and longitudinal (b) to the flow direction in the plate. [Color figure can be viewed in the online issue, which is available at wileyonlinelibrary.com.]

Table II. List of the Thickness and the Glass Fiber Content and the Nickname

Matrix material	Thickness h (mm)	Glass fiber mass content Ψ (–)	Used naming convention (thickness_fiber content)
PA6	1.5/3/4/5	0	1.5_0/3_0/4_0/5_0
PA6	1.5/3/4/5	0.15	1.5_15/3_15/4_15/5_15
PA6	1.5/3/4/5	0.30	1.5_30/3_30/4_30/5_30
PA6	1.5/3/4/5	0.40	1.5_40/3_40/4_40/5_40

moisture absorption in the 4 mm squares takes place in accordance with the behavior of Fick's law. In the thinner (1.5 mm) squares, an overshoot of the increasing mass is noted for both the 85 and 50% humidity levels [see Figure 3(a)]. A plateau in absorption exists between 96 and 480 h of climate storage before a further increase in mass occurs for a humidity level of 50%, which is presumably after 1000 h not yet complete. A decrease of the mass within the 1000 h of climate storage is only observed at a high relative humidity of 85%. The difference between the maximum moisture absorption depending on the thickness in the same climate condition is very low at 50% RH and 10% RH as compared to 85% RH.

If squares with a thickness of 1.5 and 4 mm are subjected to a climate condition of 65°C and 85% RH (see Figure 5), an overshoot of the increasing mass is not only observed at a thickness of 1.5 mm, but also in 4 mm thick specimens. The moisture absorption itself exhibits Fick's behavior with two different

Table III. Parameters of Climate Storage

Temperature ϑ (°C)	Relative humidity φ_{RH} (%RH)	Referenced standard
85	85	IEC 60068-2-78: Environmental testing—Part 2-78: Tests—Test Cab: Damp heat, steady state[28]
85	50	IEC 60068-2-2: Environmental testing—Part 2-2: Tests—Test B: Dry heat[29]
85	10	IEC 60068-2-2: Environmental testing—Part 2-2: Tests—Test B: Dry heat[29]
65	85	IEC 60068-2-78: Environmental testing—Part 2-78: Tests—Test Cab: Damp heat, steady state[28]
65	50	IEC 60068-2-2: Environmental testing—Part 2-2: Tests—Test B: Dry heat[29]
40	85	IEC 60068-2-78: Environmental testing—Part 2-78: Tests—Test Cab: Damp heat, steady state[28]
−40	-	IEC 60068-2-1: Environmental testing—Part 2-1: Tests—Test A: Cold[30]

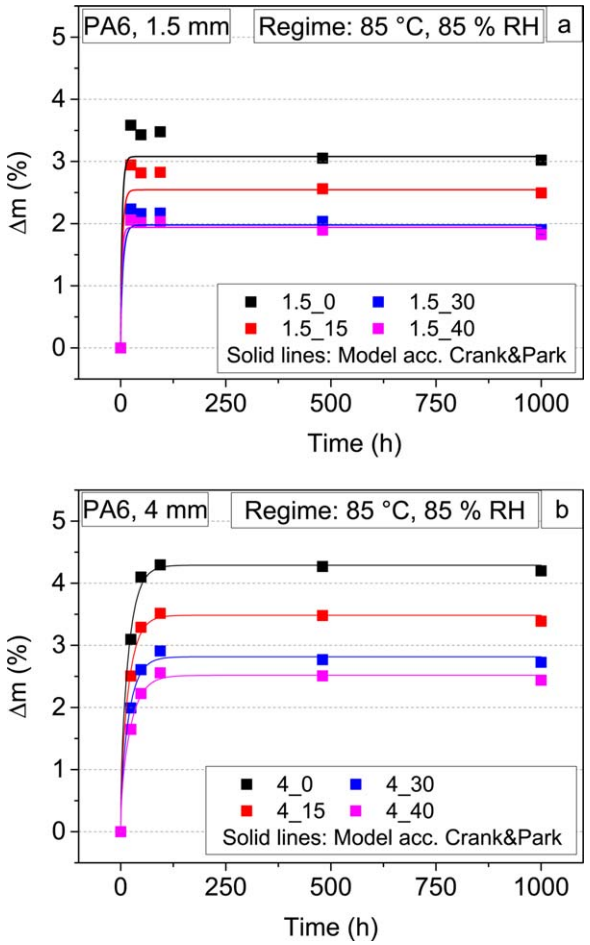

Figure 3. Relative mass change Δm at 85°C and 85% RH for squares with 1.5 mm (a) and 4 mm (b) thickness depending on glass fiber content, the solid line curves according model by Crank and Park.[1] [Color figure can be viewed in the online issue, which is available at wileyonlinelibrary.com.]

ranges. To emphasize these two ranges, two different diffusion coefficients are determined, one for 0–96 h and one for 0–1000 h. The first diffusion coefficient is characteristic of a strong increase in the relative mass change within 96 h while also considering the overshooting mass increase. The second diffusion coefficient characterizes the state of equilibrium which is achieved after 480 h. The calculated parameters are shown in

Table IV. Parameters of Modeling Curve in Figure 3

Variant of specimen	Δm_{1000h} (%)	M_e (%)	D (mm²/s)
1.5_0	3.02	3.08	14.54×10^{-6}
1.5_15	2.50	2.54	12.26×10^{-6}
1.5_30	1.90	1.98	9.67×10^{-6}
1.5_40	1.83	1.94	17.58×10^{-6}
4_0	4.20	4.29	19.6×10^{-6}
4_15	3.39	3.48	19.3×10^{-6}
4_30	2.73	2.82	18.4×10^{-6}
4_40	2.44	2.52	15.5×10^{-6}

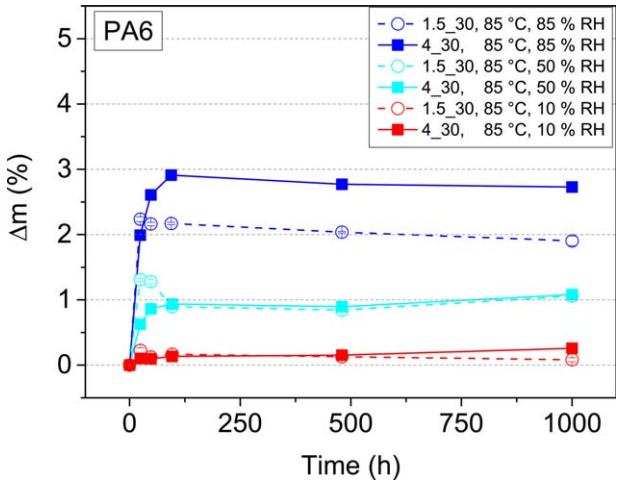

Figure 4. Relative change in mass as a function of the thickness 1.5 and 4 mm at 85°C and 85% RH, 50% RH and 10% RH. [Color figure can be viewed in the online issue, which is available at wileyonlinelibrary.com.]

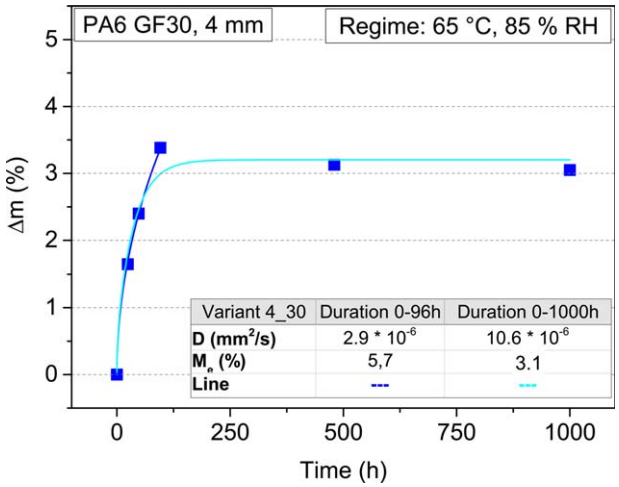

Figure 6. Relative change in mass of the variant 4_30 at 65°C and 85% RH with fit curves of the calculated diffusion coefficients. [Color figure can be viewed in the online issue, which is available at wileyonlinelibrary.com.]

Figure 6, where the calculated coefficients are also represented as solid lines. The diffusion coefficients differ by a factor of approximately 3 and the calculated relative mass change at equilibrium differs by approximately a factor of 2. As compared to 85°C and 85% RH, the equilibrium state is slightly higher, and the additional weight loss after reaching the maximum moisture

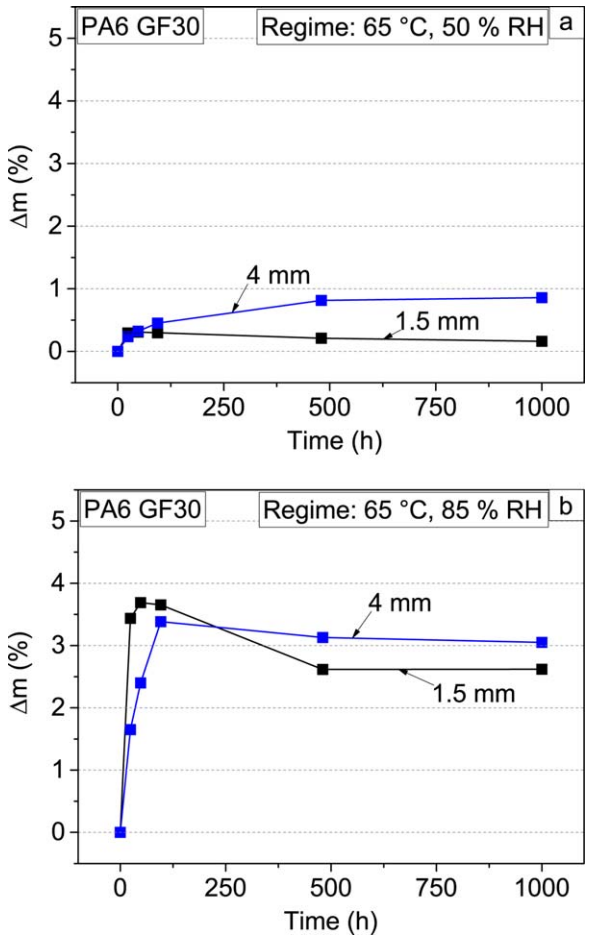

Figure 5. Relative change in mass as a function of the thickness 1.5 and 4 mm at 65°C and 50% RH (a) and 65°C and 85% RH (b). [Color figure can be viewed in the online issue, which is available at wileyonlinelibrary.com.]

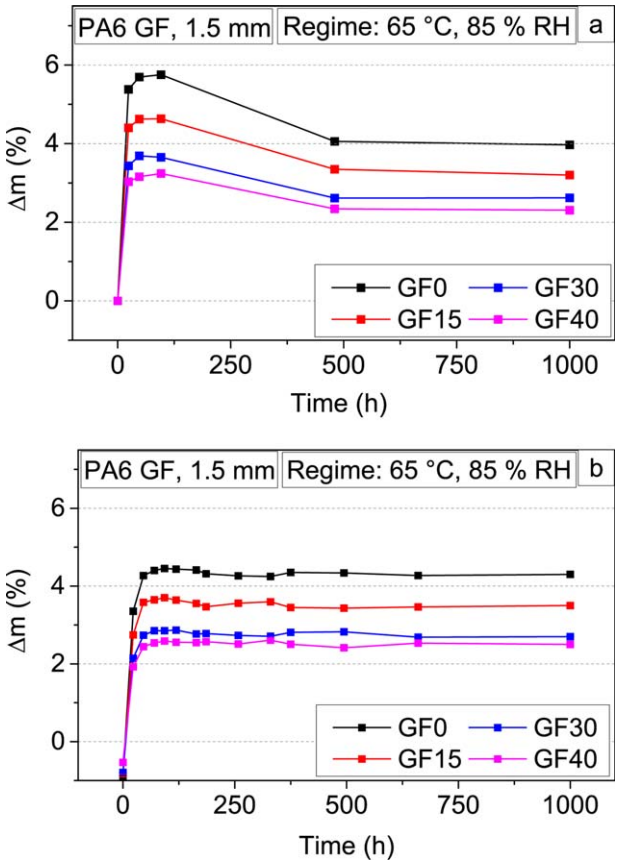

Figure 7. Overshooting mass increase of 1.5 mm thickness as a function of glass fiber content at 65°C and 85% RH (a) and after drying at 50°C and re-exposing the same samples to 65°C, 85% RH (b). [Color figure can be viewed in the online issue, which is available at wileyonlinelibrary.com.]

absorption (as shown in Figure 3) is only observed at a thickness of 4 mm.

The influence on the increase in mass in a climate condition of 65°C and 50% RH, as shown in Figure 5, can be compared to the results at 85°C and 50% RH (Figure 4) with respect to the maximum absorption of moisture. An overshoot of the increasing mass is present at 1.5 mm thickness to a small extent. However, at 4 mm thickness moisture absorption occurs more slowly, due to the reduced concentration gradient and the lower temperature.

There was little difference in the values of mass increase after 1000 h of climate storage for temperature ranges between 40 and 85°C. However, the influence of relative humidity on the mass change was considerably higher. This confirms the data of Vlasveld *et al.*, who have reported an increased dependence on the maximum moisture absorption on the relative humidity at constant temperature using unreinforced PA6 and PA6/Silicate Nanocomposite.[23]

Investigation of the Overshooting Mass Increase

It is apparent from Figures 3, 4, and 5 that at certain climatic conditions there is an overshooting of increasing mass due to the moisture absorption. This has already been observed by Low *et al.*,[14] Foulc *et al.*,[15] and Guermazi *et al.*[16] in the moisture absorption of semicrystalline polymers (polyamide PA6/clay nanocomposites, polyethylene terephthalate PET, HDPE high density polyethlyen). If the overshoot is defined as the difference between the temporary maximum of the increase in mass and the saddle point or the state of equilibrium of the relative change in mass, it can be observed that the largest difference occurs at climate conditions of 65°C and 85% RH, and a sample thickness of 1.5 mm. In Figure 7, the increase in mass at this climate condition is shown. Fick's behavior can be assumed for the first 96 h of climate storage, thereafter a decrease in mass to the equilibrium state follows. If the same squares are dried after the first climate storage at 50°C and then re-exposed to the same climatic conditions, the overshoot in mass is not observed. This indicates that during the first climate storage, a rapid diffusion in the peripheral regions of the squares takes place, in which fiber content is lower and less crystalline regions are present.[36–39] The different crystallization depending on the thickness and the cooling process during injection molding, as well as the diffusing water molecules, allow post crystallization of these marginal areas and also allow a subsequent displacement of the water molecules. In this work, a difference in crystallization of 3.1% at a dry state between the surface and core of the material was determined, with the higher value in the core region.[38]

In Figure 8, the effects of this overshooting mass increase (Δm_{os}) as a function of temperature (40, 65, and 85°C), relative humidity (10% RH, 50% RH, and 85% RH), thickness (1.5, 3, and 4 mm) and glass fiber content (0, 15, 30, 40%) are shown. As can be seen from Figure 8, a gradation depending mainly on the thickness and glass fiber content for each climate condition exists. Overall the overshoot of increasing mass was greatest in climate conditions of 65°C and 85% RH. Nevertheless, a small overshoot effect could be observed in climate conditions of 85°C and 85% RH and 50% RH, and at 65°C and 50% RH,

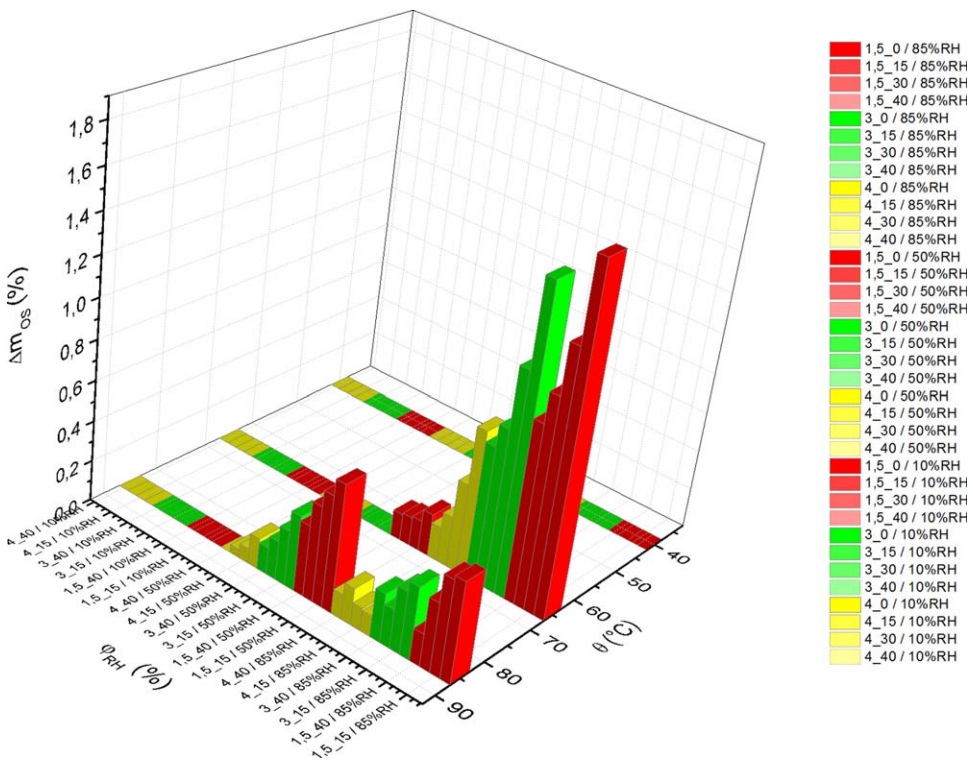

Figure 8. 3D illustration of the effect of overshooting mass increase as a function of temperature, relative humidity, thickness, and fiber content. [Color figure can be viewed in the online issue, which is available at wileyonlinelibrary.com.]

whereas at a relative humidity of 10%, as expected, no overshoot occurred. At 65°C and 50% RH, an overshoot was observed at a thickness of 1.5 mm. It can be assumed that an overshoot of increasing mass in semicrystalline polymers generally takes place when the test specimen, due to the production process, comprise multiple layers and thus has different ranges of crystallization and of fiber distribution, as was described by Woelfel *et al.*[36,37,39] Furthermore, moderate temperatures above the glass transition range and a high relative humidity of greater or equal to 50% are necessary. According to Woelfel, 5% of the thickness represents a surface layer. In the current work, a surface layer of 0.228 at 4 mm thickness and of 0.042 mm at 1.5 mm thickness were determined for PA6/GF30 with the MicroCT.

Effect of the Moisture Absorption and the Simultaneous Postcrystallization on Material Volume and Geometry

Due to the described increase in mass, there are changes in the material's volume and geometry. It cannot generally be assumed that the relative change in volume proportionally follows the relative mass change, since other factors, including the climatic conditions, thickness, and fiber content of the squares significantly influence the aging processes. This is shown in Figure 9(a,b) which illustrate the relative change in volume with respect to the relative change of mass for squares of thickness 1.5 mm (a) and 4 mm (b) at three different temperatures and at a constant relative humidity of 85% RH. Both graphs show that at a temperature of 40°C the increase in mass causes an increase in volume. However, at a thickness of 4 mm and a temperature of 65°C or 85°C the relationship between mass and volume is not highly correlated, unlike at a temperature of 40°C. This can be explained by the fact that although a further (slight) increase in mass occurs, the volume change slows down and eventually declines due to the effect of the postcrystallization processes. The values of the DSC are listed for 85°C and 85% RH in Table V.

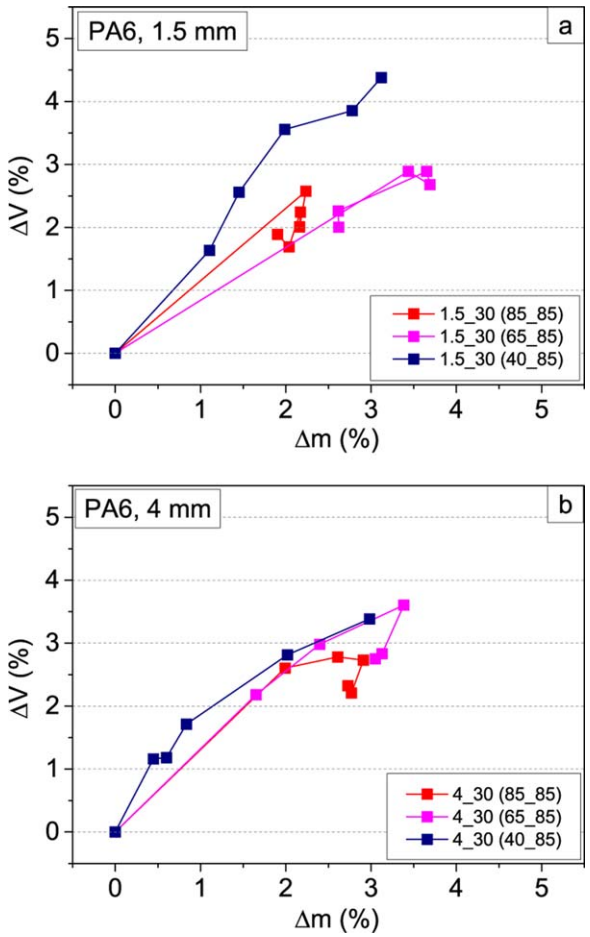

Figure 9. Relative change in volume in dependence on the relative mass at various temperatures and at constant relative humidity of 85% for 1.5 mm (a) and 4 mm (b) thick specimens. [Color figure can be viewed in the online issue, which is available at wileyonlinelibrary.com.]

At a thickness of 1.5 mm it can be seen that, after reaching a maximum mass, a contraction of the volume takes place, which occurs firstly at 85°C with almost no loss in mass. In contrast, at 65°C the loss of volume and mass occur simultaneously. Assuming that the change in volume can be directly allocated to the geometry of length *l*, width *w*, thickness *h* and furthermore that the non-reinforced PA6 reaches the equilibrium state in an environment of 40°C and 85% RH, the isotropic behavior of the change in geometry, based on swelling can be described in Figure 10 for a thickness of 4 mm. Since the moisture absorption after 1000 h has not yet reached the state of equilibrium, the expansion in the longitudinal and transverse directions has not been completed [Figure 9(a,b)] and is lagging the change in thickness. Extrapolating from the recorded data, a value of between 1.8 and 2% can be assumed, which corresponds to the value of the thickness change. For the values of the anisotropic PA6/GF-materials the expansion is dependent on the fiber orientation. Thus, the expansion after 1000 h for PA6/GF30 amounts to 0.4% in the main fiber orientation and 0.6% in the transverse orientation.

The thickness increases from between 2 and 2.7% depending on the fiber content, in which the PA6/GF generally expands more in the flow direction than unreinforced PA6, as will be discussed later in this publication. This effect tends to confirm the results reported by Thomason for PA66/GF after aging in water and antifreeze.[4,7] In these studies, it was found that the thickness expands more than the length and width and that this change in thickness amounts to approximately 60% of the volume change. The effects of overshoot in increasing mass can be seen in geometric changes when exposed to a climate condition of 65°C and 85% RH (see Figure 9). In this case, the overshoot in all three directions as a function of thickness and fiber content can be observed.

As shown in Figure 10 in the diagrams (a) change in length, (b) change in width, and (c) change in thickness, unreinforced PA6 in the equilibrium state shows nearly isotropic expansion behavior, that is, the expansion caused by the injection induced molecular orientation is either very low or it is superimposed by other processes such as swelling. However, at the start of the climate storage the overshoot is particularly noticeable in the thickness dimension. For the material PA6/GF an anisotropic expansion behavior can also be detected in these climatic

Table V. Degree of Crystallinity Compared New versus Aged for PA6 and PA6/GF30

Time (h)	PA6 4_0	PA6/GF30 4_30
0	25.6%	25.6%
1000	29.2%	25.8%

conditions. Along the flow direction of the injection molding expansion of approximately 0.4% occurs. Expansion of approximately 0.6% occurs in the direction transverse to the fiber orientation. The fiber content has very little influence on the expansion in length but more influence on the expansion in width. The expansion of the thickness as shown previously at PA6/GF is greater than at unreinforced PA6. Expansions in all three directions behave similarly in climate conditions of 85°C and 85%, and 65°C and 85% RH.

Chemical degradation, which was investigated by using SEC, leads to a small increase in molecular mass (mass average molar mass $\bar{M}_w$) at 85°C, 10% RH due to post polymerization (+3.1% at PA6/GF), and to a slight decrease of molecular mass at 85°C, 85% RH due to hydrolysis (−8.0%) which confirms the results reported by Kohan,[21] and Becker and Braun.[22] Neither aging processes have any influence on dimensional stability within the investigated climatic range.

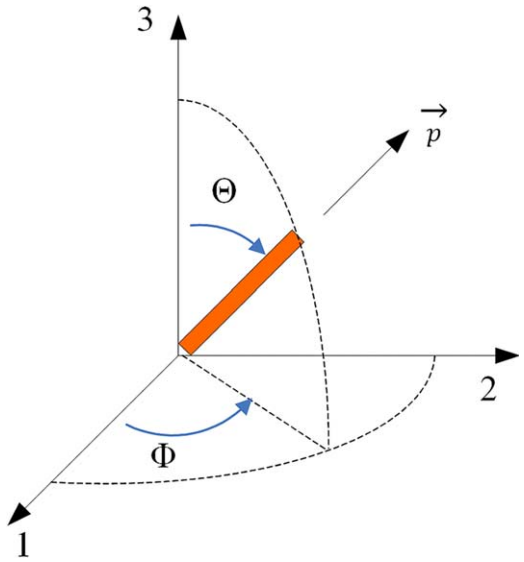

Figure 11. Representation of the solid angle with respect to axis name by Advani and Tucker.[40] [Color figure can be viewed in the online issue, which is available at wileyonlinelibrary.com.]

Correlation of the Glass Fiber Orientation to Geometry Changes

Consideration of the glass fiber orientation (fiber orientation distribution, FOD) can be given to mathematical models by

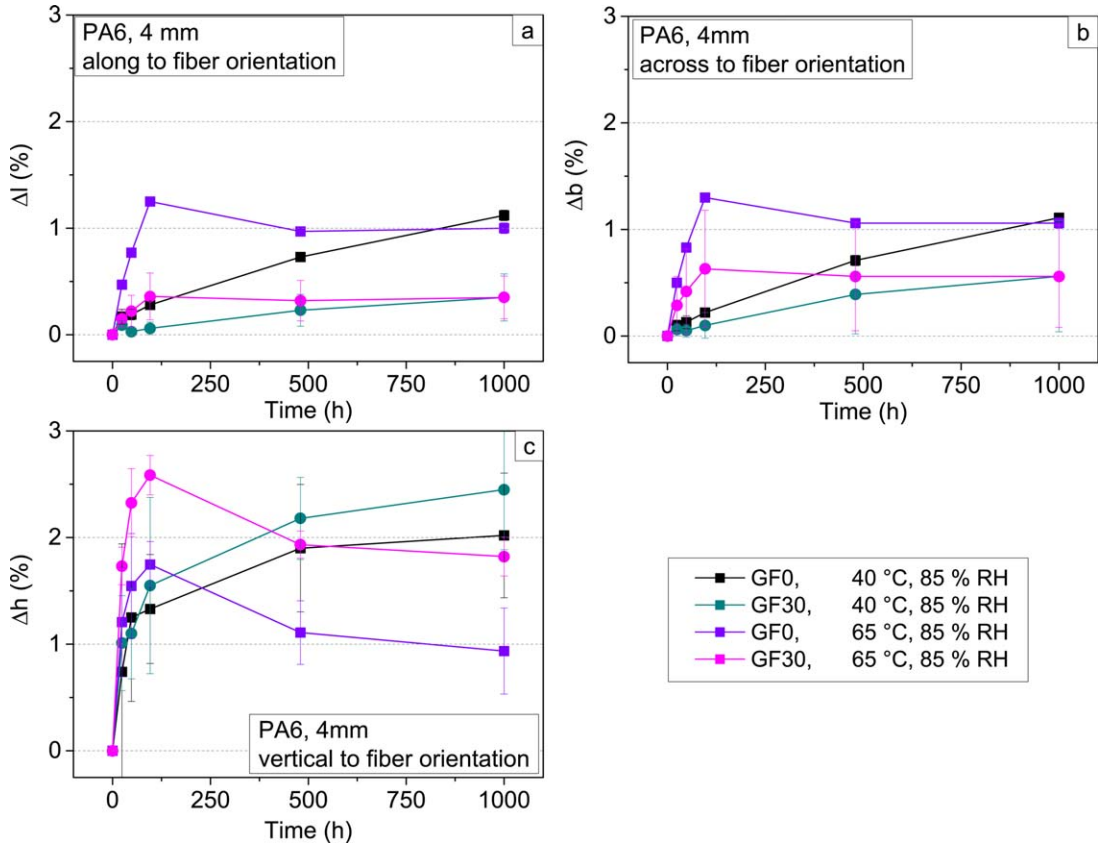

Figure 10. Geometric change in squares with 4 mm thickness in three directions at 40 and 65°C at constant 85% RH as a function of glass fiber content and orientation, (a) along, (b) transverse, and (c) vertical to the fiber orientation. [Color figure can be viewed in the online issue, which is available at wileyonlinelibrary.com.]

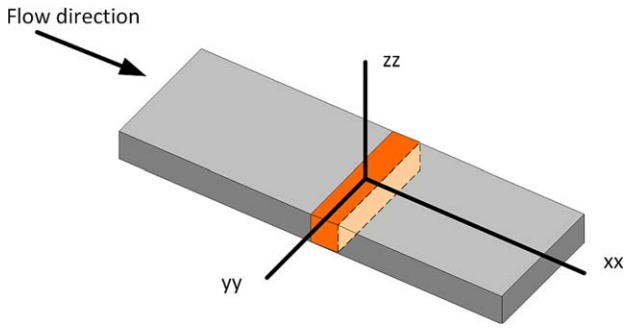

Figure 12. Representation of the MicroCT analyzed area and the corresponding Cartesian coordinate system. [Color figure can be viewed in the online issue, which is available at wileyonlinelibrary.com.]

using a tensor description of the second stage, as presented by Advani and Tucker.[40] Equation (6) is based on a contour integral and describes the relationship between the fiber orientation in a 3D range [see Figure 11 and eq. (5)] with a probability function Ψ.

$$p_1 = \sin\Theta\cos\Phi \tag{5a}$$

$$p_2 = \sin\Theta\sin\Phi \tag{5b}$$

$$p_3 = \cos\Theta \tag{5c}$$

$$a_{ij} = \oint p_i p_j \Psi(p,t)\delta p \tag{6}$$

By using MicroCT and subsequent software analysis the average glass fiber orientations were determined. The orientations can be represented by the tensor second stage $\boldsymbol{T}_{\mathrm{FOD}}$ as shown in eq. (7), which describes the glass fiber orientation in the Cartesian coordinate system. The indices used (*xx*, *yy*, and *zz*) are the principal axes in the coordinate system based on the MicroCT representation (see Figure 12).

$$\boldsymbol{T}_{\mathrm{FOD}} = \begin{bmatrix} a_{xx} & & \\ & a_{yy} & \\ & & a_{zz} \end{bmatrix} \tag{7}$$

Based on the normalization of the tensor $\boldsymbol{T}_{\mathrm{FOD}}$ it follows that $a_{xx} + a_{yy} + a_{zz} = 1$. Furthermore the number of components of the tensor can be reduced due to symmetry conditions from 9 to 6.[41–43] Due to this symmetry in the manufacturing process the analysis of the glass fiber orientation could be limited to the middle section of the multipurpose test specimen at positions 1, 3, and 5 of the injection-molded plate (see Figure 2), due to the symmetry in the manufacturing process. For a specimen thickness of 4 mm and a glass fiber content of 30% the values for a_{xx}, a_{yy}, a_{zz} were determined as 0.68, 0.24, and 0.07. The other tensor components were omitted since their values were negligible. The calculated values of the fiber orientation in the flow direction (a_{xx}) agree with the values that were presented by O'Gara *et al.*[43] (avg a_{xx} = 0.8), Thomason[44–46] (avg a_{xx} = 0.55–0.8) and Bernasconi and Cosmi[47] (avg a_{xx} = 0.65–0.83) in their works. The characteristic behavior of expansion of PA6/GF in climates of 85°C and 85% RH (see Figure 3) and 65°C and 85% RH (see Figure 5), depends

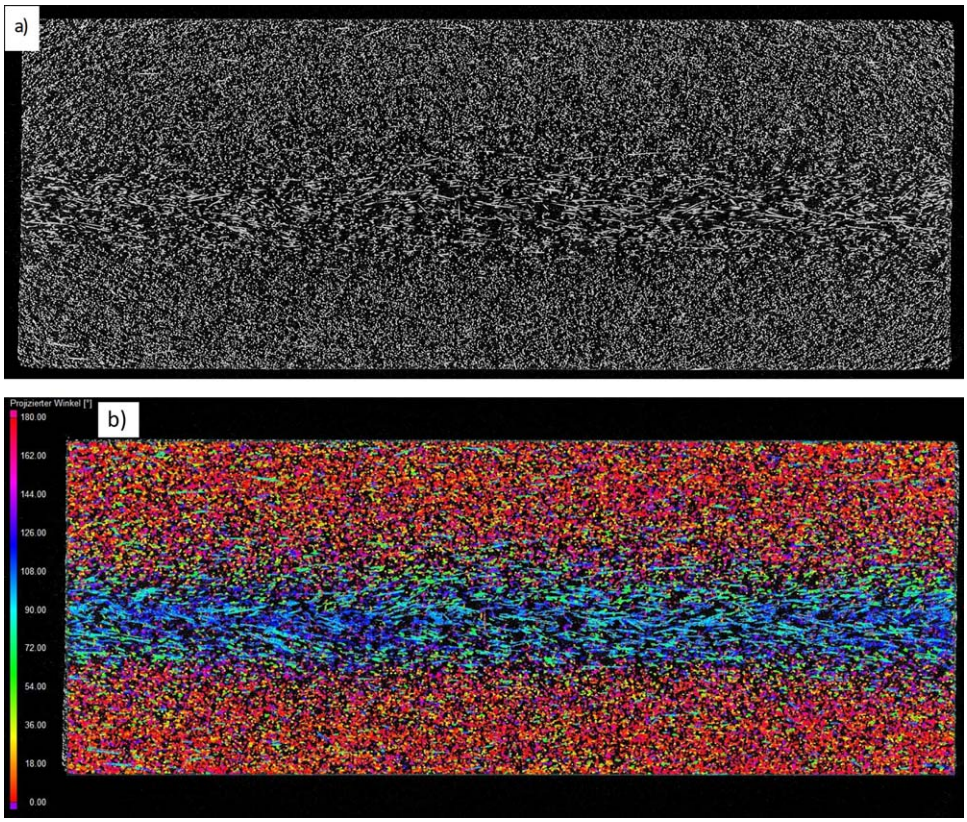

Figure 13. *X–Z* projection of the glass fiber orientation of the specimen 4_30 position 3 (a) after computer tomography, (b) after software analysis with VOLUME GRAPHICS STUDIO MAX V2.2. [Color figure can be viewed in the online issue, which is available at wileyonlinelibrary.com.]

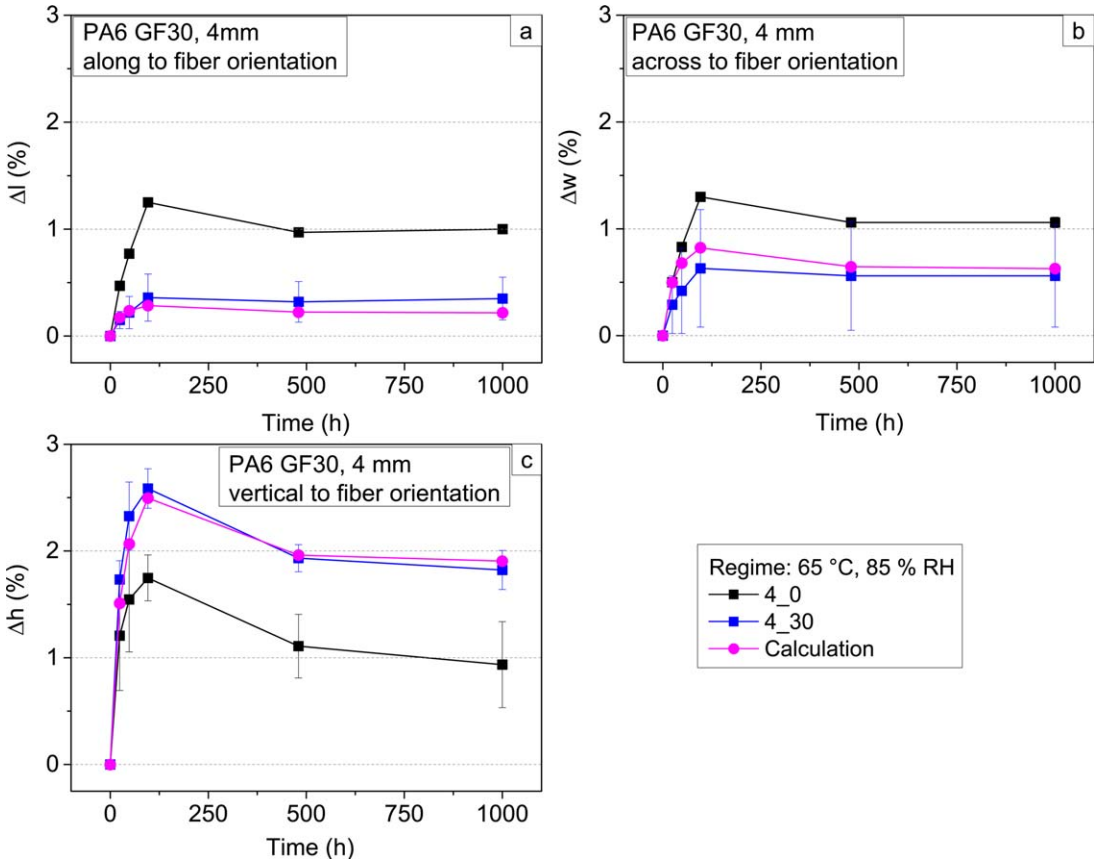

Figure 14. Geometric change in three axes of the squares 4_0 and 4_30 at 65°C and 85% RH, comparison of real measuring points to approximation. [Color figure can be viewed in the online issue, which is available at wileyonlinelibrary.com.]

on the thickness and the glass fiber content. As already mentioned, the expansion of the thickness of glass fiber reinforced PA6/GF material is always greater than the comparable thickness change in unfilled PA 6 materials. Starting from an isotropic volume change for unreinforced PA6 materials it should be noted that the expansion of each direction is limited in PA6/GF materials mainly by the fiber orientation along this axis. Since the hygroscopic behavior of PA6/GF could not be prevented but only limited, the prevented expansion of *xx*- and *yy* direction takes place in the *zz* direction (i.e. thickness, according to Figure 12). Since the actual glass fibers are oriented preferably in the plane *xx–yy* due to injection molding (see Figure 13), the expansion of the *zz* direction ought to be weighted lower in an approximation. The mathematical relationship is shown in eqs. (8–11). Since this is an approximation, the symbols are marked with the tilde operator ∼.

$$\tilde{\Delta}l = \frac{\Delta v}{3} \cdot a_{yy} \tag{8}$$

$$\tilde{\Delta}b = \frac{\Delta v}{3} \cdot \Delta a_{xx} \tag{9}$$

$$\tilde{\Delta}d = \Delta v - \frac{\Delta v}{3} \cdot a_{yy} - \frac{\Delta v}{3} \cdot a_{xx} \tag{10}$$

In summary, the following matrix calculation based on the orientation tensor can be set-up to approximate the expansion:

$$\begin{bmatrix} \tilde{\Delta}b & & \\ & \tilde{\Delta}l & \\ & & \tilde{\Delta}d \end{bmatrix} = \begin{bmatrix} a_{xx} & & \\ & a_{yy} & \\ & & a_{zz}+2 \end{bmatrix} \cdot \frac{\Delta v}{3} \tag{11}$$

In Figure 13, the glass fiber orientation angles are shown in color, as they were determined with VOLUME GRAPHICS STUDIO MAX v2.2 in a sectional view. In the core zone it can be clearly seen that the main orientation is within the plane transverse to the flow direction, which was also reported by Bernasconi and Cosmi.[47] Above and below the core zone, the glass fiber orientations are not unique to one direction, but are distributed. This distribution is also evident from the components of the orientation tensor.

If the expansions are determined based on the change in volume with the help of the modified orientation tensor [eq. (11)], for squares with a thickness of 4 mm thickness and 30 wt % glass fiber content under climate conditions of 65°C and 85% RH, the results are in good accordance with the actual measurement points (see Figure 14). However, in a climate storage of 85°C and 85% RH the results show a relative difference of about 20% between real points and approximated points for expansion in length and width and a variation of about 10% between real points and approximated points for thickness.

CONCLUSIONS

The aim of this work was both the assessment of moisture absorption in PA6 materials with different test specimen thicknesses, glass fiber contents, and fiber orientations, as well as the analysis of the effect of different climatic conditions on the dimensional stability of the test specimens. For this purpose, extensive studies were carried out. It was demonstrated that the moisture uptake of short glass fiber reinforced PA6/GF-materials at high temperatures and high relative humidity agree with Fick's law only for squares of thickness of at least 4 mm. For the thin squares (1.5–3 mm) both a higher moisture absorption rate and a subsequent decrease in mass were observed. These changes are a result of the increasing mass overshoot. For reduced relative humidity and temperature this characteristic material behavior could be confirmed, in principle. At the beginning of climate storage Fick's behavior was observed only for thicker squares, whereas for the thinner squares increasing mass overshoot occurs. The moisture absorption depends in particular on the relative humidity and less on the temperature, thickness or fiber content. In contrast, the increasing mass overshoot is dependent on both the temperature as well as on the relative humidity, and is significantly influenced by the material thickness and glass fiber content. The effect is most evident at a temperature of 65°C and a relative humidity of 85%. A linear relationship between weight gain and the change in volume could not be determined at a temperature of 85°C. The changes in the length, width and thickness are dependent on the climate conditions as well as the thickness, degree of crystallization and glass fiber orientation. Finally, the expansion of PA6/GF materials due to moisture uptake takes place to a larger extent in a direction perpendicular to the flow direction and can be correlated with the glass fiber orientation.

ACKNOWLEDGMENTS

The authors wish to thank BASF SE Ludwigshafen, Germany for providing the material and for implementation of the MicroCT analysis and the SEC analysis and Polymer Service GmbH Merseburg, Germany for conducting the experiments.

REFERENCES

1. Crank, J.; Park, G. *J. Chem. Soc. Farad. Trans.* **1951**, *47*, 1072.
2. Park, G. S.; Crank, J. Diffusion in Polymers; Academic Press: London, **1968**.
3. Starkweather, H. W. *J. Appl. Polym. Sci.* **1959**, *2*, 129.
4. Thomason, J. L.; Porteus, G. *Polym. Compos.* **2011**, *32*, 639.
5. Thomason, J. *Polym. Compos.* **2007**, *28*, 344.
6. Bergeret, A.; Pires, I.; Foulc, M.; Abadie, B.; Ferry, L.; Crespy, A. *Polym. Test.* **2001**, *20*, 753.
7. Thomason, J.; Ali, J. *Compos. Part A: Appl. Sci.* **2009**, *40*, 625.
8. Thomason, J. L.; Porteus, G. *Polym. Compos.* **2011**, *32.9*, 1369.
9. Thomason, J.; Ali, J.; Anderson, J. *Compos. Part A: Appl. Sci.* **2010**, *41*, 820.
10. Ishak, Z.; Berry, J. *J. Appl. Polym. Sci.* **1994**, *51*, 2145.
11. Martin, J. R.; Gardner, R. J. *Polym. Eng. Sci.* **1981**, *21*, 557.
12. Valentin, D.; Paray, F.; Guetta, B. *J. Mater. Sci.* **1987**, *22*, 46.
13. Carrascal, I.; Casado, J.; Polanco, J.; Gutiérrez-Solana, F. *Polym. Compos.* **2005**, *26*, 580.
14. Low, H.; Liu, T.; Loh, W. *Polym Int.* **2004**, *53*, 1973.
15. Foulc, M.; Bergeret, A.; Ferry, L.; Ienny, P.; Crespy, A. *Polym. Degrad. Stabil.* **2005**, *89*, 461.
16. Guermazi, N.; Elleuch, K.; Ayedi, H. *Mater. Des.* **2009**, *30*, 2006.
17. Bergeret, A.; Ferry, L.; Ienny, P. *Polym. Degrad. Stab.* **2009**, *94*, 1315.
18. Lyons, J. S. *Polym. Test.* **1998**, *17*, 237.
19. Langer, B. Bruchmechanische Bewertung von Polyamid-Werkstoffen, Ph.D. Thesis Martin-Luther-Universität Halle-Wittenberg, Merseburg, **1997**.
20. Monami, A.; Reincke, K.; Grellmann, W.; Kretzschmar, B. *J. Appl. Polym. Sci.* **2013**, *128*, 1885.
21. Kohan, M. I. Nylon Plastics Handbook; Carl Hanser Verlag: Munich, **1995**.
22. Becker, G. W.; Braun, D. Kunststoff-Handbuch 3. Thermoplaste 4. Polyamide; Carl Hanser Verlag: München, **1998**.
23. Vlasveld, D.; Groenewold, J.; Bersee, H.; Picken, S. *Polymer* **2005**, *46*, 12567.
24. Hernandez, R. J.; Gavara, R. *J. Polym. Sci. Pol. Phys.* **1994**, *32*, 2367.
25. BASF SE, Ultramid (PA) Product Brochure, Ludwigshafen, Germany, **2010**.
26. ISO 3167, Plastics—Multipurpose Test Specimens, **2014**.
27. ISO 294-3, Plastics—Injection Moulding of Test Specimens of Thermoplastic Materials—Part 3: Small Plates, **2002**.
28. IEC 60068-2-78, Environmental Testing—Part 2–78: Tests—Test Cab: Damp heat, steady state, **2012**.
29. IEC 60068-2-2, Environmental Testing—Part 2-2: Tests—Test B: Dry heat, **2007**.
30. IEC 60068-2-1, Environmental Testing—Part 2-1: Tests—Test A: Cold, **2007**.
31. ISO 1183-1, Plastics—Methods for determining the density of non-cellular plastics—Part 1: Immersion method, liquid pyknometer method and titration method, **2012**.
32. ISO 11357-1, Plastics—Differential Scanning Calorimetry (DSC)—Part 1: General principles, **2009**.
33. Xenopoulos, A.; Wunderlich, B. *J. Polym. Sci. Polym. Phys.* **1990**, *28*, 2271.
34. Atkins, P. W.; De Paula, J. Physikalische Chemie, 4th ed.; Wiley VCH Verlag: Weinheim, **2006**.
35. Boukhoulda, B.; Adda-Bedia, E.; Madani, K. *Compos. Struct.* **2006**, *74*, 406.
36. Wölfel, U. Verarbeitung faserverstärkter Formmassen im Spritzgießprozess, Ph.D. Thesis RWTH Universität Aachen, **1987**.

37. Wübken, G. Einfluss der Verarbeitungsbedingungen auf die innere Struktur thermoplastischer Spritzgussteile unter besonderer Berücksichtigung der Abkühlverhältnisse, Ph.D. Thesis RWTH Aachen, **1974**.

38. Illing, T. Bewertung von mechanischen und thermischen Eigenschaften glasfaserverstärkter Polyamid-Werkstoffe unter besonderer Berücksichtigung des Alterungsverhaltens von Bauteilen in der Automobilindustrie, PhD Thesis (in preparation) Martin-Luther-Universität Halle-Wittenberg.

39. Seltzer, R.; Frontini, P. M.; Mai, Y.-W. *Compos. Sci. Technol.* **2009**, *69*, 1093.

40. Advani, S. G.; Tucker, III, C. L. *J. Rheol.* **1987**, *31*, 751.

41. Bay, R. S.; Tucker, C. L. *Polym. Compos.* **1992**, *13*, 317.

42. Bay, R. S.; Tucker, C. L. *Polym. Compos.* **1992**, *13*, 332.

43. O'Gara, J. F.; Novak, G. E.; Wyzgoski, M. G. 10th-Annual SPE® Automotive Composites Conference and Exhibition (ACCE), Sept 15–16 2010, Troy, Michigan, **2010**.

44. Thomason, J. *Polym. Compos.* **2006**, *27*, 552.

45. Thomason, J. *Compos. Part A: Appl. S.* **2008**, *39*, 1732.

46. Thomason, J. *Compos. Sci. Technol.* **2001**, *61*, 2007.

47. Bernasconi, A.; Cosmi, F. *Proc. Eng.* **2011**, *10*, 2129.